On the large eddy simulation of turbulent flows in complex geometry

By S. Ghosal

1. Motivation and objectives

Application of the method of LES to a turbulent flow consists of three separate steps. First, a filtering operation is performed on the Navier-Stokes equations to remove the small spatial scales. The resulting equations that describe the space-time evolution of the 'large eddies' contain the subgrid-scale (sgs) stress tensor that describes the effect of the unresolved small scales on the resolved scales. The second step is the replacement of the sgs stress tensor by some expression involving the large scales — this is the problem of 'subgrid-scale modeling'. The final step is the numerical simulation of the resulting 'closed' equations for the large scale fields on a grid small enough to resolve the smallest of the large eddies, but still much larger than the fine scale structures at the Kolmogorov length. In dividing a turbulent flow field into 'large' and 'small' eddies, one presumes that a cut-off length δ can be sensibly chosen such that all fluctuations on a scale larger than δ are 'large eddies' and the remainder constitute the 'small scale' fluctuations. Typically, δ would be a length scale characterizing the smallest structures of interest in the flow. In an inhomogeneous flow, the 'sensible choice' for δ may vary significantly over the flow domain. For example, in a wall bounded turbulent flow, most statistical averages of interest vary much more rapidly with position near the wall than far away from it. Further, there are dynamically important organized structures near the wall on a scale much smaller than the boundary layer thickness. Therefore, the minimum size of eddies that need to be resolved is smaller near the wall. In general, for the LES of inhomogeneous flows, we must consider the width of the filtering kernel δ to be a function of position. If a filtering operation with a nonuniform filter width is performed on the Navier-Stokes equations, one does not in general get the standard large eddy equations. The complication is caused by the fact that a filtering operation with a nonuniform filter width in general does not commute with the operation of differentiation. This is one of the issues that we have looked at in detail as it is basic to any attempt at applying LES to complex geometry flows. Our principal findings are summarized in this report. For details the reader is referred to Ghosal and Moin, 1993.

In the field of subgrid-scale modeling, a large effort was invested in research on the dynamic localization model. The theoretical fundamentals have been set out in detail in our last report (Ghosal, Lund & Moin, 1993). In this report, we present some further results of tests performed on the model. These tests are on homogeneous turbulence, but tests on wall bounded flows have also been conducted by other members of the LES group and will be presented elsewhere (see the report by Cabot in this volume).

2. Accomplishments

This section is divided into two parts. In §2.1, we summarize the theoretical work on the derivation of the basic LES equations for flows requiring nonuniform grids. In §2.2, some results from the ongoing tests of the dynamic localization model are presented.

2.1 The basic equations for the LES of turbulent flows in complex geometry

2.1.1 Nonuniform filtering in one space dimension (definition)

Consider a field $\phi(\xi)$ defined in the domain $(-\infty, +\infty)$. A filtering operation with a constant filter width Δ is defined by (Leonard, 1974)

$$\bar{\phi}(\xi) = \frac{1}{\Delta} \int_{-\infty}^{+\infty} G\left(\frac{\xi - \eta}{\Delta}\right) \phi(\eta) d\eta \tag{1}$$

where G is any function with domain $(-\infty, +\infty)$ and endowed with the following properties:

(i) $G(-\xi) = G(\xi)$
(ii) $\int_{-\infty}^{+\infty} G(\xi) d\xi = 1$
(iii) $G(\xi) \to 0$ as $|\xi| \to \infty$ sufficiently fast so that all moments

$$\int_{-\infty}^{+\infty} G(\xi) \xi^n d\xi$$

$(n \geq 0)$ exist.
(iv) $G(\xi)$ is very small (in some suitably defined sense) outside $(-\frac{1}{2}, +\frac{1}{2})$.

Some examples of possible filter functions are the 'top-hat' filter

$$G(\xi) = \begin{cases} 1, & \text{if } |\xi| \leq \frac{1}{2}; \\ 0, & \text{otherwise} \end{cases} \tag{2}$$

and the 'Gaussian' filter

$$G(\xi) = \sqrt{\frac{2}{\pi}} \exp(-2\xi^2). \tag{3}$$

(For a discussion of the various types of filters used in LES, see Aldama, 1990.)

In situations where the domain might be finite or semi-infinite and a variable filter width is desirable, the definition (1) can have many possible generalizations. For example, a generalization of (1) when G is the top-hat filter might be

$$\bar{\phi}(\xi) = \frac{1}{(\Delta_+(\xi) + \Delta_-(\xi))} \int_{\xi - \Delta_-(\xi)}^{\xi + \Delta_+(\xi)} \phi(\eta) d\eta \tag{4}$$

where $\Delta_+(\xi)$ and $\Delta_-(\xi)$ are positive functions and $\Delta_+(\xi) + \Delta_-(\xi)$ is the effective filter width at location 'ξ'. For a finite or semi-infinite domain, $\Delta_+(\xi)$ and $\Delta_-(\xi)$

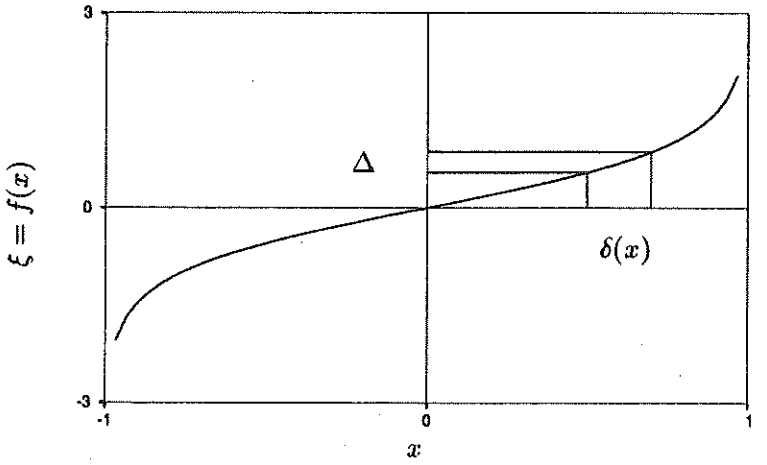

FIGURE 1. The space x, with variable filter width $\delta(x)$, is shown mapped into a space ξ, with constant filter width Δ, by the 'tan-hyperbolic map' $f(x) = \tanh^{-1} x$.

must go to zero at the boundaries sufficiently rapidly so that $(\xi - \Delta_-(\xi), \xi + \Delta_+(\xi))$ is always in the domain of ϕ.

A filtering operation with a nonuniform filter width (such as the one defined in (4)) does not in general commute with the operation of differentiation. It may be shown (Moin *et al.*, 1978), for example, that with the definition (4),

$$\overline{\frac{d\phi}{d\xi}} - \frac{d\bar{\phi}}{d\xi} = \frac{\frac{d}{d\xi}(\Delta_+(\xi) + \Delta_-(\xi))}{\Delta_+(\xi) + \Delta_-(\xi)}\bar{\phi} - \frac{1}{(\Delta_+ + \Delta_-)}\left[\phi(\xi + \Delta_+)\frac{d\Delta_+}{d\xi} + \phi(\xi - \Delta_-)\frac{d\Delta_-}{d\xi}\right]. \tag{5}$$

Thus,

$$\left(\overline{\frac{d\phi}{d\xi}}\right) \neq \frac{d\bar{\phi}}{d\xi}. \tag{6}$$

One would like to believe that the right-hand side of (5) would be small for some reasonable class of nonuniform filters, but this has never been conclusively demonstrated. This lack of commutativity between filtering and differentiation causes every spatial derivative operator in the Navier-Stokes equations to generate terms that cannot be expressed solely in terms of the filtered fields. Therefore, a 'closure problem' is introduced not only for the nonlinear terms, but for the linear terms as well. To remedy this situation we first propose an alternate definition for the filtering operation that is more general than (4).

Let ϕ be some field defined in a finite or infinite domain $[a, b]$. Any nonuniform grid in the domain $a \leq x \leq b$ can be mapped to a uniform grid of spacing Δ in the domain $[-\infty, +\infty]$ by means of some mapping function

$$\xi = f(x). \tag{7}$$

Here $f(x)$ is a monotonic differentiable function such that

$$f(a) = -\infty, \tag{8}$$

$$f(b) = +\infty. \tag{9}$$

The nonuniform grid spacing $\delta(x)$ is clearly given by

$$\delta(x) = \frac{\Delta}{f'(x)} \tag{10}$$

(see figure 1). Clearly, if a (or b) is finite, (8)-(9) requires $f'(a)$ (or $f'(b)$) to be infinite so that $\delta(a)$ (or $\delta(b)$) $= 0$. Since $\delta(x)$ can be regarded as a 'local' filter width (see equation (16)), the filtering kernel becomes a Dirac delta function at finite boundaries. This, of course, is an ideal limit that in a practical numerical computation can be achieved only approximately. Thus, our stipulation that the grid spacing be approximately equal to the filter width must break down when we are sufficiently close to a wall because in practice one cannot have an infinitely dense clustering of grid points at the boundary.

The filtering operation is defined as follows. Given an arbitrary function $\psi(x)$, we first make a change of variables to ξ to obtain the new function $\phi(\xi) = \psi(f^{-1}(\xi))$. The function $\phi(\xi)$ is then filtered using the usual definition (1) appropriate for filtering on a uniform grid. Finally, we transform back to the variable x. Thus,

$$\bar{\psi}(x) \equiv \bar{\phi}(\xi) = \frac{1}{\Delta}\int_{-\infty}^{+\infty} G\left(\frac{f(x)-\eta}{\Delta}\right)\phi(\eta)d\eta, \tag{11}$$

or, on using (7), we have

$$\bar{\psi}(x) = \frac{1}{\Delta}\int_{a}^{b} G\left(\frac{f(x)-f(y)}{\Delta}\right)\psi(y)f'(y)dy. \tag{12}$$

Equation (11) or, equivalently, (12) is the definition we shall adopt for the filtering operation with a nonuniform filter width. For reasons that will become apparent in the next section, we will call this the Second Order Commuting Filter (SOCF). It should be noted that the definition (4) used by Moin *et al.* is quite different from what one would get on substituting the expression (2) for the top-hat filter into (12).

Example: In channel flow, one often uses the 'tanhyperbolic grid' (see for example Moin & Kim, 1982. The mapping function discussed below is slightly different from the version actually used in numerical computations since there one uses only a finite number of grid points whereas our filters become infinitely sharp at the walls).

$$f(x) = \tanh^{-1} x \tag{13}$$

where $+1 \geq x \geq -1$. ($x = \pm 1$ correspond to the channel walls.) From equation (12), the filtering operation is defined as

$$\bar{\psi}(x) = \int_{-1}^{+1} \tilde{G}(x,y)\psi(y)dy \tag{14}$$

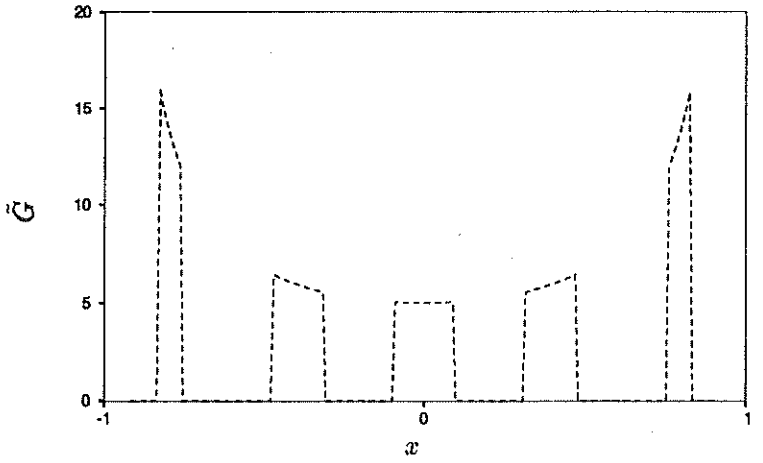

FIGURE 2A. The shape of the filter function $\tilde{G}$ when G is a top-hat filter.

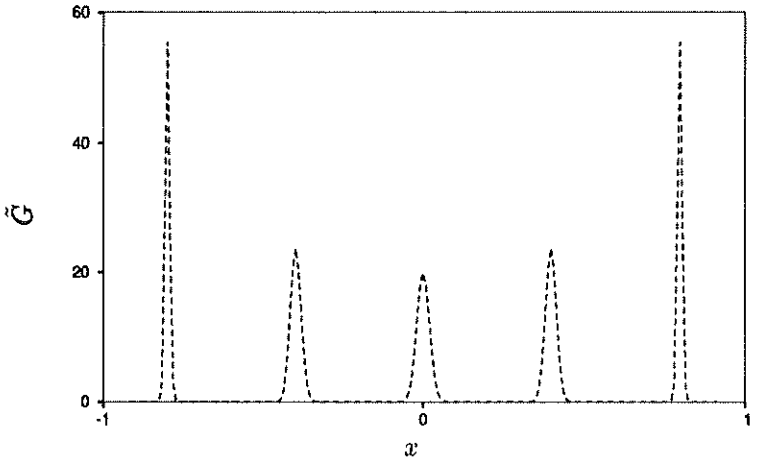

FIGURE 2B. The shape of the filter function $\tilde{G}$ when G is a Gaussian filter.

where

$$\tilde{G}(x,y) = \frac{1}{\Delta} G\left(\frac{f(x)-f(y)}{\Delta}\right) f'(y) \tag{15}$$

with $f(x) = \tanh^{-1} x$. The function $\tilde{G}(x,y)$ is plotted in figure 2A when G is a top-hat filter and in figure 2B when G is a Gaussian filter. If the approximations $f(x)-f(y) \approx f'(x)(x-y)$ and $f'(y) \approx f'(x)$ for y near x are used in (15), we have on using (10)

$$\tilde{G}(x,y) \approx \frac{1}{\delta(x)} G\left(\frac{x-y}{\delta(x)}\right). \tag{16}$$

Thus, as a first approximation, the filtering kernel $\tilde{G}$ contracts in a self-similar manner on approaching a finite boundary (see figures 2 A and B). However, the exact

formula (15) has an additional higher order effect that causes the filter function $\tilde{G}$ to become asymmetric near the wall giving more weight to points nearer the wall than further from it. The effect is most clearly seen in figure 2A.

2.1.2 Calculation of the commutation error

Let us define the commutation error as

$$C[\psi] \equiv \left(\overline{\frac{d\psi}{dx}}\right) - \frac{d\bar{\psi}}{dx} \tag{17}$$

Then it is easily shown that

$$C[\psi] = \frac{1}{\Delta}\int_a^b G\left(\frac{f(x)-f(y)}{\Delta}\right)\psi'(y)f'(y)\left[1-\frac{f'(x)}{f'(y)}\right]dy. \tag{18}$$

(The boundary terms are strictly zero due to the conditions (8) and (9).)

It is convenient to introduce the new variable ζ such that y is expressed implicitly in terms of ζ through the equation

$$f(y) = f(x) + \Delta\zeta \tag{19}$$

Equation (19) can be inverted by expressing y in a power series

$$y = y_0(\zeta) + \Delta y_1(\zeta) + \Delta^2 y_2(\zeta) + \cdots \tag{20}$$

where $y_0(\zeta)$, $y_1(\zeta)$, $\cdots$ are functions to be determined. On substituting (20) in (19) and equating like powers of Δ, one obtains the expansion

$$y = x + \frac{\Delta\zeta}{f'} - \frac{\Delta^2 f''}{2f'^3}\zeta^2 + \cdots. \tag{21}$$

(Note: When the argument of any function is omitted, we imply that the function is evaluated at 'x'.) In terms of ζ, equation (18) may be written as

$$C[\psi] = \int_{-\infty}^{+\infty} G(\zeta)\psi'(y)\left[1-\frac{f'(x)}{f'(y)}\right]d\zeta \tag{22}$$

where y is given by (21) (the limits of integration are obtained on using (8) and (9) in (19)). On expanding each of the factors in the integrand of (22) in Taylor series in Δ and collecting terms of the same order, we have,

$$C[\psi] = c_1\Delta + c_2\Delta^2 + \cdots = c_1'\delta + c_2'\delta^2 + \cdots \tag{23}$$

where

$$c_1 = \frac{f''\psi'}{f'^2}\int_{-\infty}^{+\infty}\zeta G(\zeta)d\zeta, \tag{24}$$

$$c_2 = \frac{2f'f''\psi'' + f'f'''\psi' - 3f''^2\psi'}{2f'^4} \int_{-\infty}^{+\infty} \zeta^2 G(\zeta) d\zeta, \tag{25}$$

$c_1' = c_1 f'$ and $c_2' = c_2 (f')^2$. Since $G(\zeta)$ is symmetric, $c_1 = c_1' = 0$. Thus, the commutation error $\mathcal{C}[\psi] \sim O(\delta^2)$.

In an LES, the grid spacing is approximately equal to the 'filter-width', δ. If a second order numerical scheme is used to represent the derivatives, the finite differencing error is then of the same order as the error due to the lack of commutativity of the differentiation and the filtering operations. Therefore, in an LES of an inhomogeneous turbulent flow using a second order finite differencing scheme, the filtering operation can be considered to commute with the differentiation operation to within the accuracy of the numerical approximation. This is our most important result from the point of view of practical application.

2.1.3 Spectral distribution of the commutation error

Let us substitute

$$\psi = \hat{\psi}_k \exp(ikx) \tag{26}$$

and (21) in (22). Then,

$$\mathcal{C}[\psi] = ik\psi \int_{-\infty}^{+\infty} G(\zeta) \left[1 - \frac{f'(x)}{f'\left(x + \frac{\Delta\zeta}{f'} + \cdots\right)} \right] \exp\left(ik \frac{\Delta\zeta}{f'} + \cdots \right) d\zeta. \tag{27}$$

On expanding the integrand of (27) in a power series in Δ, we have

$$\frac{\mathcal{C}[\psi]}{\psi} = \mathcal{F}_0(k\Delta) + \Delta \mathcal{F}_1(k\Delta) + \cdots \tag{28}$$

where $\mathcal{F}_0, \mathcal{F}_1, \ldots$ contain Δ only in the combination $k\Delta$.

Now $\Delta \ll 1$, but $k\Delta$ may be as large as order one. Thus, we may neglect the successive terms in (28) in comparison to the first term to obtain

$$\frac{\mathcal{C}[\psi]}{\psi} \simeq \mathcal{F}_0(k\Delta). \tag{29}$$

On evaluating $\mathcal{F}_0(k\Delta)$ from (27), we have

$$\frac{\mathcal{C}[\psi]}{\psi} = ik\Delta \frac{f''}{(f')^2} \mathcal{F}\left(\frac{k\Delta}{f'} \right) \tag{30}$$

where $\mathcal{F}$ is defined by

$$\mathcal{F}(x) = \int_{-\infty}^{+\infty} \zeta G(\zeta) \exp(ix\zeta) d\zeta. \tag{31}$$

Equation (30) can also be written as

$$\frac{\mathcal{C}[\psi]}{\psi} = -ik\delta\left(\frac{\delta'}{\delta}\right)\mathcal{F}(k\delta) \tag{32}$$

where δ is the local filter width as defined in (10). On expanding the exponential in (31) in a Taylor series, we see by virtue of $G(\zeta)$ being symmetric that $\mathcal{F}(k\delta) \sim k\delta$ so that $|\mathcal{C}[\psi]/\psi| \sim (k\delta)^2$ as shown in the last section.

Comparison with finite differencing errors is facilitated if the commutation error is expressed as a 'modified wave-number'. If $\mathcal{C}[\psi]$ were zero, we will have for the function (26)

$$\frac{d\bar{\psi}}{dx} = \overline{\frac{d\psi}{dx}} = \overline{ik\psi} = ik\bar{\psi}. \tag{33}$$

Therefore, if we define a 'modified wave-number' k' by

$$\frac{d\bar{\psi}}{dx} = ik'\bar{\psi}, \tag{34}$$

then the departure of k' from k is a measure of the commutation error. On making the change of variable (19) in (12), we obtain

$$\bar{\psi}(x) = \int_{-\infty}^{+\infty} G(\zeta)\psi(y)d\zeta. \tag{35}$$

On substituting (26) in (35) and on using the definition (34), we obtain

$$\frac{k'}{k} = \frac{\int_{-\infty}^{+\infty} G(\zeta)\exp(iky(x,\zeta))\frac{\partial y(x,\zeta)}{\partial x}d\zeta}{\int_{-\infty}^{+\infty} G(\zeta)\exp(iky(x,\zeta))d\zeta} \tag{36}$$

where y has been expressed as a function of ζ by inverting (19) for each fixed value of x. Equation (36) is an exact result. A simplified asymptotic form is obtained on substituting the expansion (21) in (36) and dropping all terms such as $\Delta(k\Delta)$, $\Delta^2(k\Delta)\cdots$ which are negligible compared to $k\Delta$. Thus,

$$\frac{k'}{k} = 1 - \Delta\frac{f''}{f'^2}\frac{\int_{-\infty}^{+\infty}\zeta G(\zeta)\exp\left(\frac{ik\Delta\zeta}{f'}\right)d\zeta}{\int_{-\infty}^{+\infty} G(\zeta)\exp\left(\frac{ik\Delta\zeta}{f'}\right)d\zeta}. \tag{37}$$

Since $G(\zeta)$ is a symmetric function, (37) simplifies to

$$\frac{k'}{k} = 1 - i\Delta\frac{f''}{f'^2}\frac{\int_{-\infty}^{+\infty}\zeta G(\zeta)\sin\left(\frac{k\Delta\zeta}{f'}\right)d\zeta}{\int_{-\infty}^{+\infty} G(\zeta)\cos\left(\frac{k\Delta\zeta}{f'}\right)d\zeta}. \tag{38}$$

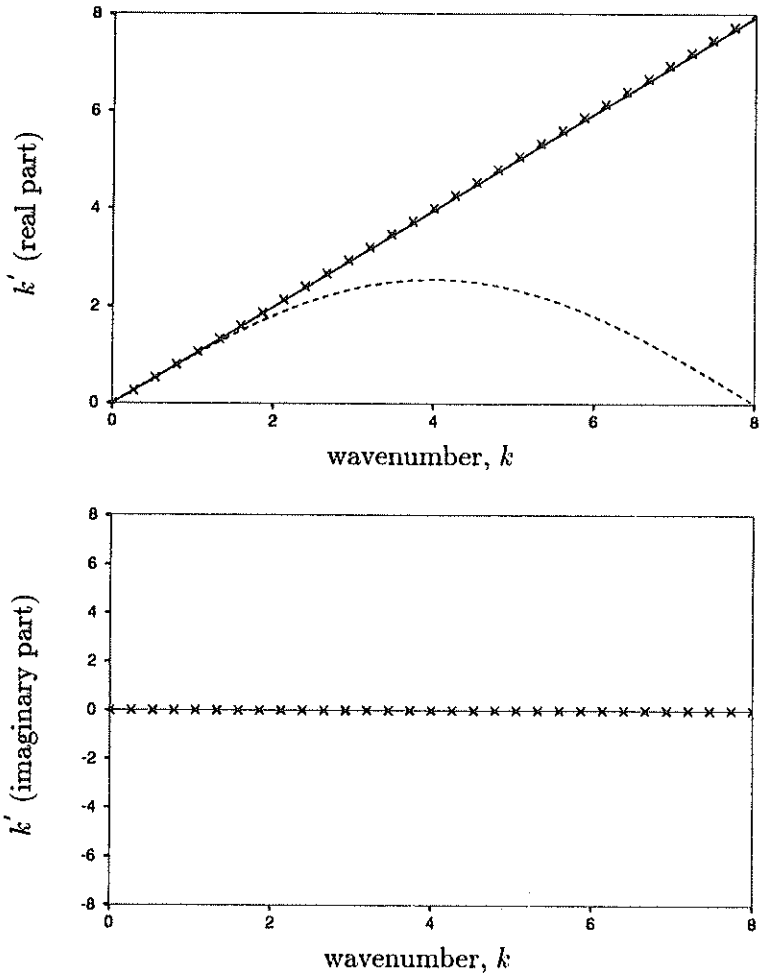

FIGURE 3A. The modified wavenumber (k') for the commutation error (——) compared to that of the central differencing error (– – –). The symbols '×' are the result of using the approximate formula (42). Here $\Delta = 2\pi/16$, $x = 0$ (channel center), and the maximum wavenumber is π/δ where δ is the local filter width.

Example : Let us consider the top-hat filter defined by (2) together with the tan-hyperbolic map $f(x) = \tanh^{-1} x$. For this map, equation (19) can be inverted to give

$$y = \frac{x + \tanh \Delta\zeta}{1 + x \tanh \Delta\zeta}. \tag{39}$$

On substituting (39) in (36), we obtain

$$\frac{k'}{k} = \frac{\int_{-\infty}^{+\infty} \exp(iky) G(\zeta) \left[\frac{1-\tanh^2 \Delta\zeta}{(1+x \tanh \Delta\zeta)^2}\right]}{\int_{-\infty}^{+\infty} \exp(iky) G(\zeta) d\zeta}, \tag{40}$$

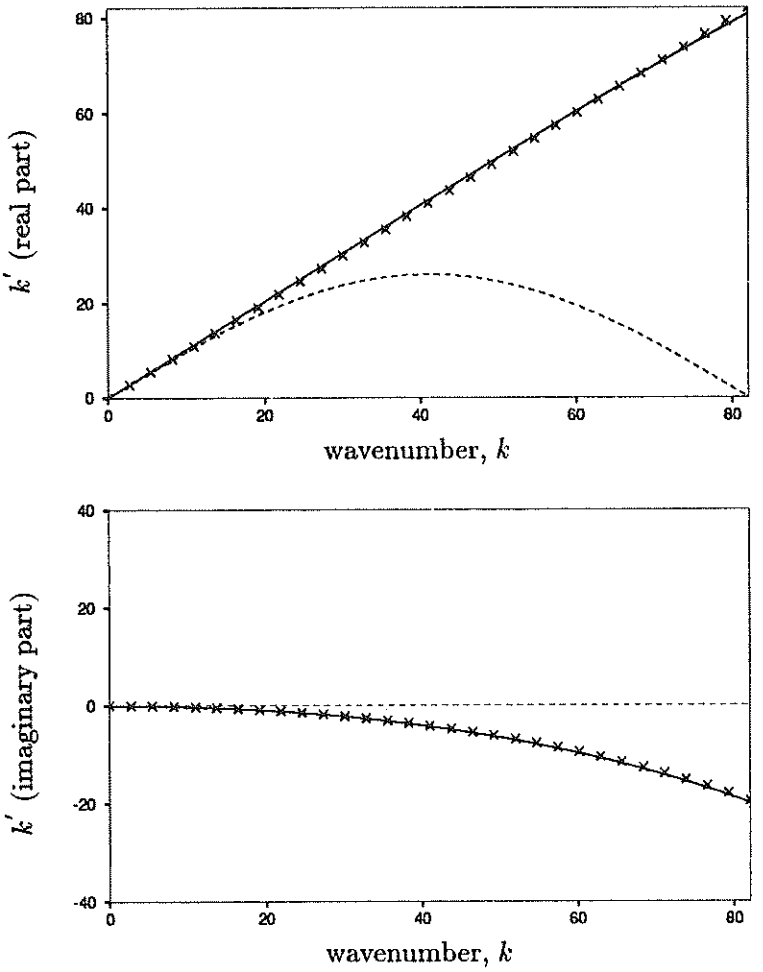

FIGURE 3B. Same as figure 3A for $x = 0.95$ (close to channel wall).

with y given by (39). As a typical example, we consider a channel whose walls are at $x = 0$ and $x = 2\pi$ with 16 grid points in the spanwise direction. Thus, $\Delta = 2\pi/16$. The integral (40) can be evaluated numerically. The result is shown in figure 3. The modified wavenumber for the second order central difference scheme is given by

$$\frac{k'}{k} = \frac{\sin(k\delta)}{k\delta}. \tag{41}$$

Equation (41) is also plotted in figure 3 for comparison. The asymptotic formula (38) can be evaluated analytically in the case of the tan-hyperbolic map and top-hat filter. A straightforward computation gives

$$k' = k + \frac{2ix}{(1-x^2)}\left[\frac{k\delta}{2}\cot\left(\frac{k\delta}{2}\right) - 1\right]. \tag{42}$$

Equation (42) is also shown in figure 3. The agreement of the asymptotic result (42) with the exact result (40) is seen to be very good.

The asymptotic formula (38) can be written in the following convenient form:

$$k_R' = k, \tag{43}$$

$$k_I' = \left(\frac{\delta'}{\delta}\right) F(k\delta) \tag{44}$$

where δ is the local filter width given by (10),

$$F(x) = x\left[\frac{\int_{-\infty}^{+\infty} \zeta G(\zeta)\sin(x\zeta)d\zeta}{\int_{-\infty}^{+\infty} G(\zeta)\cos(x\zeta)d\zeta}\right] \tag{45}$$

and the suffixes R and I denote real and imaginary parts respectively. Thus, to a very good approximation, the commutation error is seen to be purely dissipative in nature in contrast to the central differencing error, which is dispersive. The commutation error vanishes in regions where $\delta' = 0$ (such as at the center of a channel). From the example above, it is clear that for the top-hat filter,

$$F(k\delta) = 1 - \frac{k\delta}{2}\cot\left(\frac{k\delta}{2}\right) = \frac{(k\delta)^2}{12} + \frac{(k\delta)^4}{720} + \cdots. \tag{46}$$

A simple calculation shows that for the Gaussian filter (3),

$$F(k\delta) = \frac{(k\delta)^2}{4}. \tag{47}$$

2.1.4 Higher order corrections to the commutation error

We have shown in the previous section that $\mathcal{C}[\psi] \approx \psi\mathcal{F}_0(k\Delta)$ and $\mathcal{F}_0(k\Delta) \sim (k\Delta)^2$ at leading order in $k\Delta$. In this section, we shall attempt to approximate the commutation error $\mathcal{C}[\psi]$ by an expression involving $\bar{\psi}$ and its derivatives such that the residual is of order $(k\Delta)^4$. The procedure can be readily generalized to represent $\overline{\psi'(x)}$ in terms of $\bar{\psi}'(x)$ and higher derivatives of $\bar{\psi}(x)$ such that the error in the approximation is at most of order $(k\Delta)^{2m}$ where m is any positive integer.

We have, on expanding the exponential in (31) and noting that $G(\zeta)$ is a symmetric function,

$$\mathcal{F}(x) = ix\int_{-\infty}^{+\infty} \zeta^2 G(\zeta)d\zeta - \frac{ix^3}{3!}\int_{-\infty}^{+\infty} \zeta^4 G(\zeta)d\zeta + \cdots \tag{48}$$

Substitution of (48) in (30) gives

$$\mathcal{C}[\psi] = -(k\Delta)^2\frac{f''}{(f')^3}\psi\int_{-\infty}^{+\infty} \zeta^2 G(\zeta)d\zeta + O(k\Delta)^4. \tag{49}$$

From (35),

$$\bar{\psi}(x) = \int_{-\infty}^{+\infty} G(\zeta)\psi\left(x + \frac{\Delta\zeta}{f'} + \cdots\right) d\zeta. \tag{50}$$

On substituting $\psi = \hat{\psi}_k \exp(ikx)$ in (50) and differentiating twice with respect to x, we have

$$\bar{\psi}''(x) = -k^2\psi\left[1 - \alpha\frac{(k\Delta)^2}{2f'^2} + O(k\Delta)^4\right] \tag{51}$$

where

$$\alpha = \int_{-\infty}^{+\infty} \zeta^2 G(\zeta) d\zeta \tag{52}$$

and $\Delta \ll 1$ has been assumed. Equation (51) implies that

$$-k^2\psi = \bar{\psi}''(x) + O(k\Delta)^2. \tag{53}$$

On substituting (53) in (49) we get

$$C[\psi] = \alpha\frac{f''}{f'^3}\Delta^2\bar{\psi}''(x) + O(k\Delta)^4. \tag{54}$$

Thus,

$$\overline{\frac{d\psi}{dx}} = \frac{d\bar{\psi}}{dx} + \alpha\frac{f''}{f'^3}\Delta^2\frac{d^2\bar{\psi}}{dx^2} + O(k\Delta)^4. \tag{55}$$

The procedure can be continued to extend the accuracy of the representation to any order in $k\Delta$. Equation (55) can also be written in terms of the local grid spacing $\delta(x)$ as follows:

$$\overline{\frac{d\psi}{dx}} = \frac{d\bar{\psi}}{dx} - \alpha\delta^2\left(\frac{\delta'}{\delta}\right)\frac{d^2\bar{\psi}}{dx^2} + O(k\delta)^4. \tag{56}$$

Equation (56) was established only for the function (26). However, it is clearly valid for any linear superposition of functions of the type (26), that is, any function that admits a Fourier representation.

2.1.4 Generalization to three space dimensions

These results can be generalized to three space dimensions (see Ghosal and Moin, 1993 for details). Let us consider curvilinear grids defined by the co-ordinate surfaces

$$\mathbf{H}(\mathbf{x}) = constant \tag{57}$$

where $\mathbf{x}$ are rectilinear co-ordinates in physical space. Let us also introduce a new 'computational space' $\mathbf{X}$ through the map

$$\mathbf{X} = \mathbf{H}(\mathbf{x}) \tag{58}$$

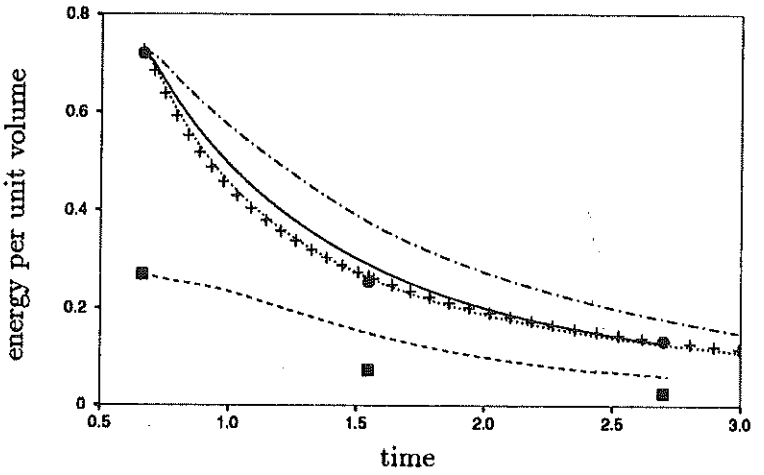

FIGURE 4A. Decay of energy in a simulation of the Comte-Bellot and Corrsin experiment with 48^3 grid points. Large scale energy (——); sgs energy (k) (– – –), as predicted by DLM(G). This is compared with an identical computation with the DLM(C) (+), the DM (· · · · · ·), and with the model turned off (—·—). Experimental: resolved energies (●); subgrid energies (■)

which maps the physical space domain into $\mathbf{R}^3$ meshed with a uniform grid of spacing Δ. The filtering operation is now defined as

$$\bar{\psi}(\mathbf{x}) = \frac{1}{\Delta^3} \int \prod_{i=1}^{3} G\left(\frac{H_i(\mathbf{x}) - H_i(\mathbf{x}')}{\Delta}\right) \psi(\mathbf{x}') J(\mathbf{x}') d^3\mathbf{x}' \tag{59}$$

where $J(\mathbf{x})$ is the Jacobian of the transformation (58).

It can be shown that for the general three dimensional filter (59), equation (54) takes the form

$$C_k[\psi] = -\alpha\Delta^2 \Gamma_{kmp} \frac{\partial^2 \bar{\psi}}{\partial x_m \partial x_p} + O(|\mathbf{k}|\Delta)^4 \tag{60}$$

where

$$\Gamma_{kmp} = h_{m,jq}(\mathbf{H}(\mathbf{x})) h_{p,q}(\mathbf{H}(\mathbf{x})) H_{j,k}(\mathbf{x}) \tag{61}$$

and $\mathbf{h}$ is the inverse of $\mathbf{H}$. Further, an expression for $C_k[\psi]$ in terms of $\bar{\psi}$ can be written down to any order in Δ. Thus,

$$\overline{\partial_k \psi} = (\partial_k - \alpha\Delta^2 \Gamma_{kmn} \partial^2_{mn} + \cdots)\bar{\psi}. \tag{62}$$

2.2 Tests of the dynamic localization model

Two versions of the dynamic localization model (DLM) were introduced in last year's Annual Research Briefs (Ghosal, Lund & Moin, 1993). The first of these

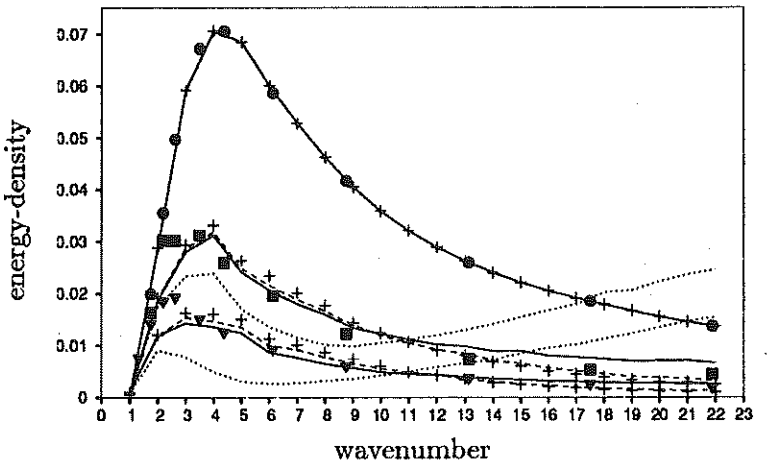

FIGURE 4B. The spectra at three times for the same computation as in figure 4A. DLM(G) (——); DM (– – –); DLM(C) (+); no model (· · · · · ·). The solid circles, squares, and triangles are the experimental values at the three experimental points in figure 4A. The initial conditions are chosen so that the spectra at the earliest time matches the experiment.

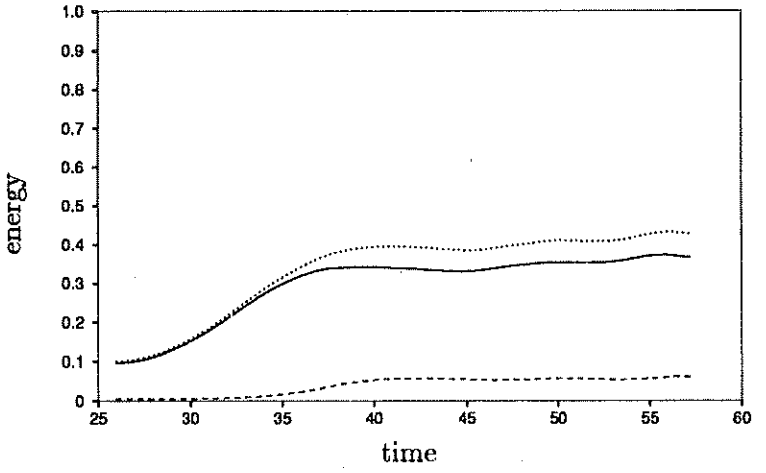

FIGURE 5A. Time dependence of energy in a forced simulation of homogeneous isotropic turbulence at infinite Reynolds number on a 32^3 grid using the DLM(G). Energy per unit volume in the resolved scales (——); subgrid-scale energy (– – –); Total energy (· · · · · ·).

(which we will call the 'constrained' dynamic localization model or DLM(C)) constrains the Smagorinsky coefficient to be nonnegative and therefore does not exhibit the phenomenon of backscatter – the (locally) reverse transfer of energy from the subgrid to supergrid scales. The second formulation (which we will call the 'general' dynamic localization model or DLM(G)) removes this restriction. However,

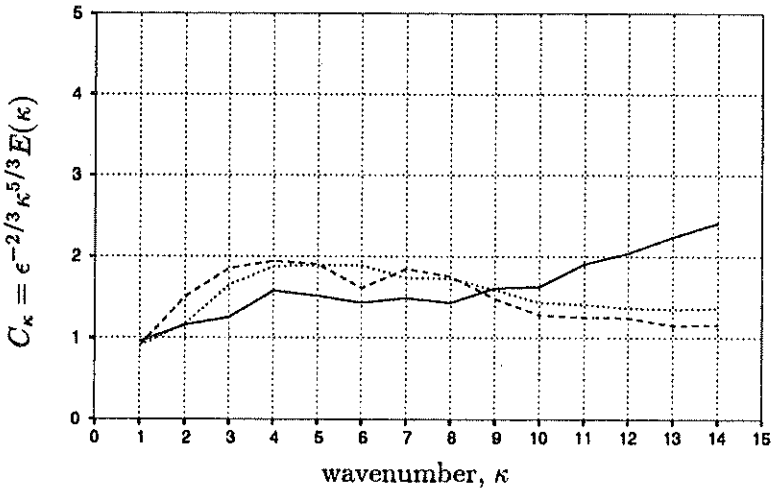

FIGURE 5B. Equilibrium spectrum in a forced simulation of homogeneous isotropic turbulence at infinite Reynolds number on a 32^3 grid. Kolmogorov's five-thirds law would correspond to a horizontal straight line with an ordinate equal to the Kolmogorov constant $C_\kappa \approx 1.5$. DLM(G) (——); DLM(C)(– – –); DM (· · · · · ·).

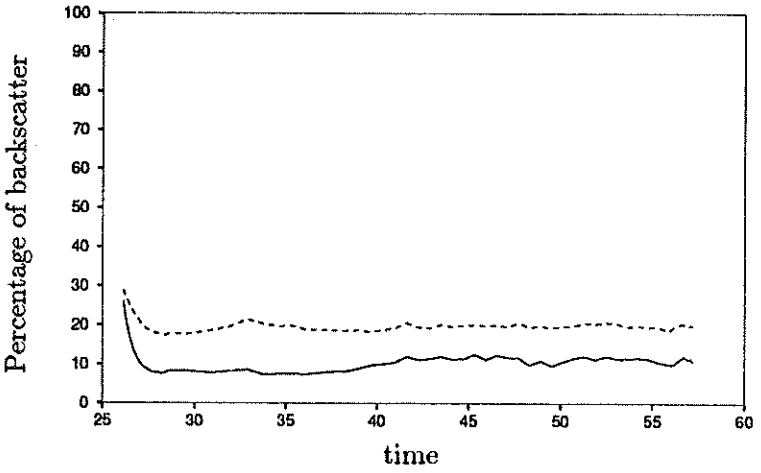

FIGURE 5C. Fraction of backscatter in a forced simulation of homogeneous isotropic turbulence at infinite Reynolds number on a 32^3 grid using DLM(G). Volume averaged rate of energy transfer from subgrid to supergrid scales as a fraction of the net transfer (——); Fraction of points experiencing backscatter at a given instant of time (– – –).

the generality is gained at the cost of added computational expense. The so called 'volume-averaged' version of the dynamic model which can be rigorously derived as a special case of the variational formulation (Ghosal, Lund & Moin, 1993) will be simply referred to as the dynamic model (DM). It is useful only for flows with

homogeneous directions.

Previous tests had shown (Ghosal, Lund & Moin, 1993) that while DLM(C) and DM used in a 32^3 LES simulation of the Comte-Bellot and Corrsin experiment (Comte-Bellot and Corrsin, 1971) gave excellent predictions, the results obtained with DLM(G) were not as satisfactory. This discrepancy was more thoroughly investigated. It was found that at a resolution of 32^3, the subgrid-scale energy (k) was almost equal to the total energy in the LES field. As such a situation is not fully consistent with the basic assumption of LES that the resolved scales carry most of the energy, the simulation was repeated on a more refined (48^3) mesh.

At this resolution the total resolved energy is about thrice the subgrid-scale energy, and the performance of the DLM(G) is greatly improved. The performance of DLM(C), DLM(G,) and DM are compared in figure 4 starting with identical initial conditions consistent with the experimental data at the initial time. All three models are seen to give comparable results in good agreement with the experiment. The result of running the simulation with the model turned off is also shown in the same figure. The crucial role played by the model in these simulations is apparent.

This was followed up with a simulation of forced homogeneous isotropic turbulence at infinite Reynolds number using a 32^3 grid. The forcing was provided by the simple artifice of resetting the six modes corresponding to $\mathbf{k} = (\pm 1, \pm 1, \pm 1)$ ($\mathbf{k}$ is the wavenumber vector) to fixed values at the end of each time-step. The achievement of steady state was monitored by plotting the energy as a function of time and also by looking for time independence in the shape of the spectra. Figure 5A illustrates the extent to which a 'steady-state' was achieved during a run using the DLM(G). Though a plateau was reached in the total energy, some oscillations remained. These could probably be reduced by running the simulation for a longer time, but part of it might be an artefact of the forcing scheme. If a strict Kolmogorov spectrum was achieved, the sgs energy would be

$$k = \int_{\kappa_m}^{\infty} C_\kappa \epsilon^{2/3} \kappa^{-5/3} d\kappa = \frac{3}{2} C_\kappa \epsilon^{2/3} \kappa_m^{-2/3} \tag{63}$$

where ϵ is the dissipation rate, κ_m is the wavenumber magnitude at cutoff, and $C_\kappa \approx 1.5$ is the Kolmogorov constant. In our simulation, $\kappa_m = 14$ (the number of full energy shells) and $\epsilon \approx 0.07$. If these numbers are substituted in (63,) we find $k \approx 0.03$. It is reassuring to note that the computed sgs energy (see figure 5A) is within a factor of two of this figure. (Of course, an accurate quantitative prediction of subgrid-scale energy cannot be expected from a large eddy simulation.)

The quantity $\epsilon^{-2/3} \kappa^{5/3} E(\kappa)$, where $E(\kappa)$ is the energy spectrum and ϵ is the sgs dissipation, is plotted in figure 5B for runs using each of the three models. No time averaging has been performed, so there is some sampling fluctuations especially at the low wavenumbers. All three models show good agreement with Kolmogorov's law with a Kolmogorov constant close to 1.5. The rising 'tail' in the DLM(G) simulation at high wavenumber appears to be real since the high wavenumber part shows negligible fluctuations among different samples. On the other hand, the DLM(G) appears to give a better plateau at intermediate wavenumbers at a value

very close to $C_\kappa \approx 1.5$. Again, this behavior was seen when the simulation was repeated with a different initial spectrum, so the effect is probably real and not just an accidental sampling fluctuation.

The percentage of 'backscatter' is shown in figure 5C using two different measures. The solid line is the rate of transfer of energy from the subgrid to supergrid scales (integrated over the volume of the box) as a fraction of the total transfer. The dashed line is the fraction of points engaged in this 'backscatter' of energy at a given time. The results on backscatter can be tested using a DNS database of a high Reynolds number simulation of homogeneous turbulence, but this has not been done yet. However, Piomelli *et al.* (1991) found, using a DNS of channel flow at $Re = 3300$, that the fraction of backscattered energy is about 10-20 percent while the fraction of backscattering points is about 20-30 percent. These numbers depend on the type of filter used. The figures quoted here are for the 'box filter' (see figure 9 in the paper of Piomelli *et al.*) which is what we are using as our 'test-filter'. Figure 5C is roughly consistent with Piomelli *et al.*'s results. These simulations were repeated using a more refined (48^3) mesh. None of the above results were changed in any significant way.

If one has to choose a model for an LES of a complex flow, then, based solely on these tests, the DLM(C) will perhaps be the model of choice since it is the simpler of the two available local models and gives results that are just as good as the more elaborate DLM(G). The extra effort invested in modeling backscatter does not seem to significantly improve predictions of quantities of practical interest. However, in more complex flow situations where backscatter is known to play an important role, the DLM(G) might turn out to be the preferred model. This issue will be settled in the near future as the results of applying these theories to complex flows become available.

3. Future plans

It is expected that these ideas will be useful in the near future in the context of the application of the dynamic localization model to LES of complex flows.

An explicit knowledge of the nature of the filtering operation was not needed in the past in sgs modeling. However, all models in the 'dynamic model' category rely on an explicit 'test' filtering operation (which is supposed to be self-similar to the grid-level filter) to extract useful information about the subgrid scales. Thus, the issue of the commutativity of the filtering and differentiation operations is important not only for providing a firm theoretical basis for LES in complex geometry, but also for practical calculations which make use of the dynamic model.

The DLM should be applied to progressively more challenging flows to evaluate its performance. Faster and more efficient algorithms for solving the relevant integral equations need to be examined.

I would like to thank Dr. Nagi Mansour for providing the basic code that was modified to do some of these tests and for his patient help in teaching the author to use it. I would also like to thank Dr. T. S. Lund for reviewing the manuscript and offering valuable suggestions.

REFERENCES

ALDAMA, A. A. 1990 Filtering techniques for turbulent flow simulation. *Lecture notes in engineering, Springer-Verlag.* **56.**

COMTE-BELLOT, G. & CORRSIN, S. 1971 Simple Eulerian time correlation of full and narrow-band velocity signals in grid-generated 'isotropic' turbulence. *J. Fluid Mech.* **48,** 273-337.

GHOSAL, S., LUND, T. S. & MOIN, P. 1993 A local dynamic model for large eddy simulation. *Annual Research Briefs-1992* Center for Turbulence Research, Stanford Univ./NASA Ames, 3-25.

GHOSAL, S. & MOIN, P. 1993 The basic equations for the large eddy simulation of turbulent flows in complex geometry. *CTR Manuscript 143.*

LEONARD, A. 1974 Energy cascade in large-eddy simulations of turbulent fluid flows. *Ad. Geophys.* **18 A,** 237-248.

MOIN, P. & KIM, J. 1982 Numerical investigation of turbulent channel flow. *J. Fluid Mech.* **118,** 341-377.

MOIN, P. & KIM, J. 1980 On the numerical solution of time-dependent viscous incompressible fluid flows involving solid boundaries. *J. Comput. Phys.* **35,** 381-392.

MOIN P., REYNOLDS, W. C. & FERZIGER, J. H. 1978 Large eddy simulation of incompressible turbulent channel flow. *Rept. no. TF12,* Dept. of Mech. Engr., Stanford University.

PIOMELLI, U., CABOT, W. H., MOIN, P. & LEE, S. 1991 Subgrid-scale backscatter in turbulent and transitional flows. *Phys. of Fluids.* **3,** 1766-1771.